Mechanical Assembly of Electrospray Thruster Grid

IEPC-2005-101

Presented at the 29th International Electric Propulsion Conference, Princeton University October 31 – November 4, 2005

B. Gassend,* L. F. Velásques-García,† A. I. Akinwande‡

and M. Martínez-Sánchez§

Massachusetts Institute of Technology, Cambridge, Massachusetts, 02139, USA

This paper presents the design and experimental validation of a method to mechanically assemble the grid of a micro-fabricated electrospray thruster array. In this method, the grid is assembled by hand by rotating it until cantilever springs engage in small notches. This method is particularly interesting as it decouples the fabrication of the grid and the rest of the thruster, permitting many different grid materials to be tried in the future, without making any changes to the process for the rest of the device. The first experiments show that a positional accuracy of 20 micrometers is possible, which is satisfactory for our application. Fabrication problems that may account for the observed misalignment are outlined.

Nomenclature

b	= finger height
d_0	= misalignment at center of grid
$d_{\max}$	= maximum misalignment across useful grid area
Δ	= maximum finger displacement during assembly
E	= Young's modulus (of silicon)
F	= clamping force from a finger at maximum displacement
F_x^1, F_y^1	= x and y component of force from one finger opposing misalignment of grid
F_x, F_y	= x and y component of total force from fingers opposing misalignment of grid
H	= width of an untapered finger
$\bar{H}$	= average width of a tapered finger
$k_\parallel$	= axial finger stiffness
$k_\perp$	= flexural finger stiffness
k	= combined stiffness of all fingers
L	= length of a finger
r	= radius of useful grid area
$\sigma_{\max}$	= maximum stress in flexed finger
t_x, t_y	= x and y component of grid translation
θ	= misalignment angle

*Research Assistant, Department of Electrical Engineering and Computer Science, 32 Vassar Street, Room 32G-838, Cambridge, MA 02139, gassend@alum.mit.edu, not an AIAA member

†Research Scientist, Department of Aeronautics and Astronautics and Microsystems Technology Laboratories, 77 Massachusetts Avenue, Room 39-657, Cambridge, MA 02139, lfvelasq@mit.edu, not an AIAA member

‡Professor, Department of Electrical Engineering and Computer Science, 77 Massachusetts Avenue, Room 39-553, Cambridge, MA 02139, akinwand@mtl.mit.edu, not an AIAA member

§Professor, Department of Aeronautics and Astronautics, 77 Massachusetts Avenue, Room 37-341, Cambridge, MA 02139, mmart@mit.edu, AIAA Senior Member

I. Introduction

In an electrospray thruster, an electrostatic field is used to extract ions or charged droplets from a liquid placed at the tip of a needle. Typically kilovolt potential differences are require to startup and run the thruster, for thrusts of micronewtons or less per needle. In order to increase thrust levels, arrays of needles must be used. Micro-fabrication techniques seem well suited to producing such arrays. To date, a number of micro-fabricated electrospray thrusters have been reported.[1,2,3,4] Planar arrays have been built and tested without a real extractor grid,[5] we want to build on that work to achieve the first complete micro-fabricated 2D electrospray thruster array.

In order to maximize the packing density of needles in the array, precise alignment between the needles and the holes in the extractor grid is needed. This alignment could be achieved by wafer bonding techniques, which involve high temperatures and lead to complexity in the fabrication process. Alternatively, for a prototype setup, the grid and needles can be fabricated separately, and aligned using a macro-scale test rig. Unfortunately, the latter technique is time consuming and prone to drift.

The main focus of this paper is a new alignment method in which the grid and the electrode can be fabricated separately, and then assembled by hand with the desired precision. In this method, the grid is held in place by a grid support system comprising a number of springs, which we will call "fingers". The person who assembles the device first roughly positions the grid into a recess on the top surface of the thruster (Figure 1(a)), and then rotates it. As the grid rotates, the shape of the grid support forces the grid to align itself to within 50 μm of the center of the thruster (Figure 1(b)). Then it begins to flex the fingers. Finally, each fingertip falls into a notch in the grid, preventing further rotation (Figure 1(c)).

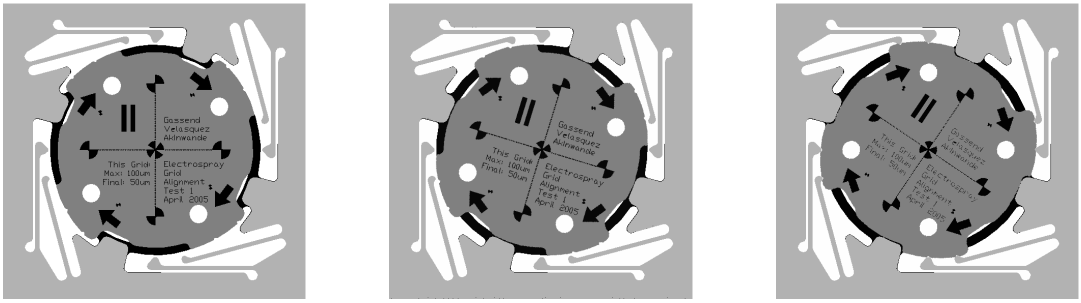

(a) The grid is placed in its recess.

(b) The grid is forced into rough alignment.

(c) The fingers precisely clamp the grid into place.

Figure 1. Hand assembly of the grid.

Once assembled, the grid is firmly held in place by the high axial stiffness of the fingers, while the lateral flexibility of the fingers allows the device to accommodate for differential thermal expansion, or consistent over/under-etching of the side-walls during processing. Moreover, with this assembly method, the processes and material selection for the grid and the rest of the thruster can be completely decoupled. For example, temperature sensitive materials like Teflon can be placed below the grid without being damaged when it is assembled (this is not possible with fusion bonding), or the material of the grid can be changed without making any other changes to the thruster.

The method we are using was directly inspired by previous work in which a system of fingers was used to assemble the grid of a linear electrospray array out of the plane of the wafer.[6] Micro-machined clips have been used by others to align and hold optical fibers,[7] to position structures perpendicular to the substrate[8] and as general purpose in-plane fasteners.[9] LEGO-like systems to align and bond wafers for packaging have been proposed.[10] Others have proposed micro-mechanical Velcro[11] to mechanically bind wafers, without providing for relative positioning of the wafers.

Figure 3(b) shows what an electrospray thruster array using this alignment method could look like. In the rest of this paper we will discuss the design, fabrication and characterization of a simple test device (shown in Figure 3(a)) comprising only a grid, a grid support, a base, and alignment marks. This test device is sufficient to evaluate the assembly method we are proposing. In Section II, we describe the design of the

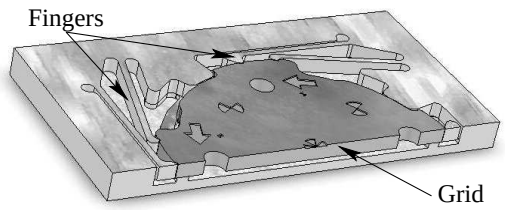

Figure 2. Section view of the device.

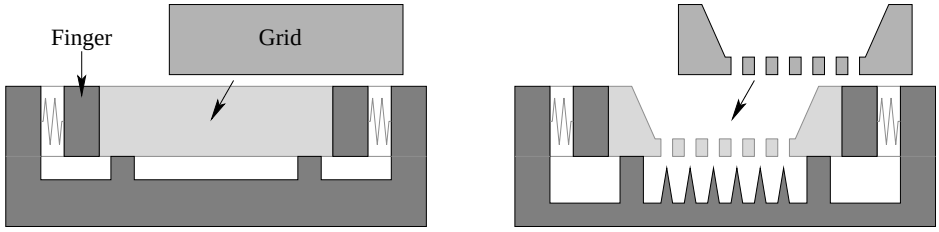

(a) Side diagram of the test device we built.

(b) Artist's view of complete thruster.

Figure 3. Our test device, and how it compares with an actual electrospray thruster.

test device. Then, in Section III we describe the process that was used to fabricate it. Finally, Section IV covers the characterization that was performed on the device once it was fabricated.

II. Device Design and Modeling

In this section we describe the design of our grid attachment method. The driving features in the design of this method were:

1. Ensure stiff and accurate location of the grid.
2. Be flexible: tolerate a range of grid materials, avoid high temperature steps at the end of the process.
3. Be robust, i.e., difficult to break, tolerant to process variation, easy to assemble.

A. Finger and Notch Design

The initial choice of a finger-based mechanical assembly method was guided by the desire for flexibility. As long as the grid has the correct shape and sufficient mechanical properties, it will be possible to assemble it.

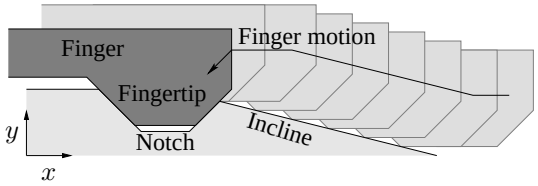

Figure 4. The motion a finger follows during assembly.

Figure 4 shows the motion a finger follows during assembly. The parts to be mated are translated relative to one another in the x direction. Initially the finger is free, then it comes into contact with the part to be

mated to. It is slowly deflected by a gentle incline, and then finally clicks into its notch. In the notch, the finger is still deflected, so there is always a force clamping the fingertip in its notch.

We place the finger so its direction of deflection is the y direction, perpendicular to the direction of relative motion of the two parts to be assembled. This prevents the clamping force from creating a systematic shift in the finger's final resting position. Moreover, the finger has low stiffness in the y direction (beam in flexion) and high stiffness in the x direction (beam in tension/compression). Thus, by placing the stiff direction of the finger parallel to the direction of assembly, we provide a high stiffness in the direction of assembly.

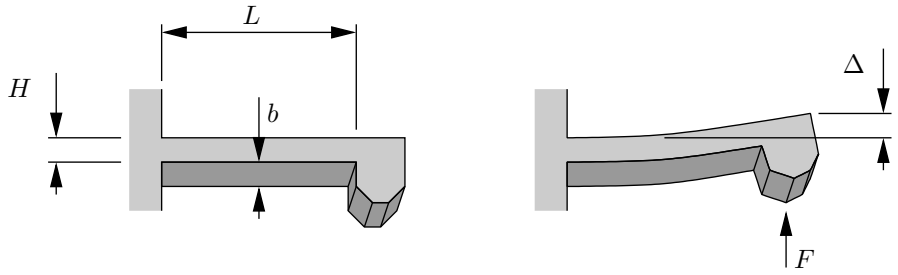

Figure 5. Notation used for describing finger geometry and flexion.

The interface between the fingertip and the notch consists in two inclined planes. The angle of inclination is the same on both sides. This way, any systematic over or under etching will change the final deflection of the fingertip, but will leave the relative x positions of the parts unchanged. For steep angles of the interface planes, a small x error translates to a large deflection in the fingers, so there is a large force trying to center the fingertip in its notch. Also, a smaller coefficient of friction is needed at the interface to prevent the finger from slipping out of its notch under the influence of a force in the x direction. However, steep walls lead to higher sensitivity to process variation since a small over or under etch corresponds to a larger change in deflection for the assembled fingertip. We chose 45° as a compromise angle for the contact plane inclinations.

The amount of motion the finger undergoes during assembly is another tradeoff. As we shall see, for a given clamping force, the finger size increases with its maximum allowable deflection. This favors small deflections. But the deflections have to be large enough to guarantee proper assembly even when process variations are considered. We have decided to be robust to over/under-etching of up to 10 μm. This means that the assembled deflection should be at least 25 μm to accommodate the worst case under-etching with 5 μm to spare. For comparison, in our fabricated devices, we have experimented with different deflections, as shown in Table 1. We have also targeted a clamping force in the hundreds of millinewtons range.

To size the fingers, we use the analysis from [6]. The notation is introduced in figure 5. We model the finger as a slender uniform cross-section beam, fixed at one end, and with a point force applied at the other end. If E is the Young's modulus of the beam, its stiffness and maximum stress $\sigma_{\max}$ are given by

$$k_{\perp} = \frac{F}{\Delta} = \frac{E\,b}{4}\left(\frac{H}{L}\right)^3 \qquad \text{and} \qquad \sigma_{\max} = \frac{3EH\Delta}{2L^2}. \tag{1}$$

Eliminating H in Eqs. (1) yields an equation that clearly shows the tradeoff between high force, large deflection and small beam length/footprint:

$$\frac{F\Delta^2}{L^3} = \frac{2\,b\,\sigma_{\max}^3}{27E^2}, \tag{2}$$

where the right hand side is only determined by the substrate we use to make the fingers. For a 650 μm thick silicon wafer, $b = 650$ μm and $E = 145$ GPa.[12] Limiting the maximum stress to a very conservative value[13] of $\sigma_{\max} < 100$ MPa, we find that $F\Delta^2/L^3 < 2.3$ mN/m.

In our design, we wanted to fit 6 devices on a 6" wafer, which limits the finger length to about a centimeter. We opted for a maximum displacement of 100 μm. Equation (2) then limits the force to about 0.2 N, and Eqs. 1 give the corresponding slenderness ratio $L/H \approx 20$. The actual final dimensions we settled on for our uniform cross section fingers were $L = 1.09$ cm, and $H = 550$ μm.

The limitations imposed by Eq. (2) only apply for uniform cross-section beams. Improved tradeoffs are possible for tapered beams, which are thick near their base and skinny further out where the moment is

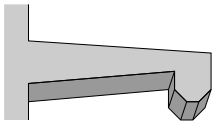

Figure 6. A linearly tapered beam.

reduced. In the optimal beam geometry, the maximum stress is reached all along the beam, and the beam width H goes like the square root of the distance to the point where the force is applied. For simplicity, we have considered linearly tapered fingers (Figure 6). We found that the best tradeoff was when H decreases by 71% across the finger. We fabricated two different tapered finger sizes (Table 1). The type I finger is 700 μm wide at its base, and can provide the same force as the linear beam (type II) with 50% extra deflection. The type III finger is limited to 100 micrometer deflections, but nearly three times as stiff as the linear beam.

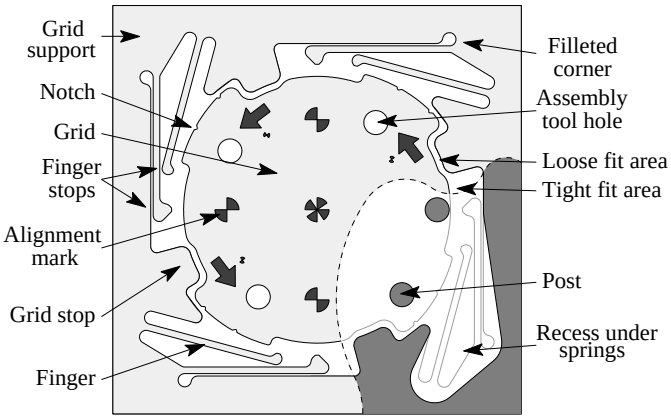

Figure 7. Major features of the assembly system. Part of the top layer has been cut away.

B. Maximizing Robustness

Now that we understand how to design fingers, we can use them to build a robust assembly system. First, we have chosen to assembly the grid by a circular motion, with a number of benefits. If there are 3 or more fingers, then as long as the fingertips remain seated in their notches, the stiffness of the grid will be determined by the axial stiffness of the fingers, as opposed to the much lower flexural stiffness. Moreover, in the circular configuration, the grid is held only by fingers (as opposed to the linear case where it could be supported by a hard contact on one side as in [6]). Thus, any systematic over/under etching, or any differential thermal expansion, simply causes the grid to appear slightly larger or smaller than expected. This change in size can be accommodated by flexing the fingers with no first order error in grid position.

The most fragile part of this device is the long slender fingers. They are flexible, but can only tolerate a few hundreds of micrometers deflection. Whenever possible we have tried to protect them from accidental damage. The reader can use Figure 7 to identify the features we shall now describe, and Figure 1 to follow the assembly steps. The first line of defense is to place the fingers on the grid holder, where they are better sheltered than they would be on the periphery of the grid. This keeps them protected until assembly time. When the grid is first placed within the grid support, the person who is assembling only needs to place it to within about half a millimeter of its intended location for it to fall into the same plane as the grid support. From this position, the grid can be wiggled around without risk to the fingers, as grid stops prevent it from coming into contact with the fingers. As the grid is rotated into place, the parts of the grid near the grid stops get wider, forcing the grid into alignment to within 50 μm, making it impossible to wiggle the grid

beyond the breaking point of the fingers. The grid stops also prevent the grid from being rotated backward, or more than 50 μm past the normal assembled position. Moreover, the fingers are placed so that if they are excessively deflected outward, they will hit a hard stop (finger stop), preventing them from flexing farther and breaking. We have also tried to maximize the grid strength by avoiding sharp corners throughout the design. Finally, in case some fingers do break, we have decided to have 8 fingers per device for redundancy.

C. Expected Performance

We have mentioned that our clamping method offers a high clamping stiffness. Indeed, consider that the grid undergoes a small translation (t_x, t_y), and assume that the fingertips remain in their notches without buckling or snapping. The force that is exerted by a finger with an axis along the x direction is determined by the axial and flexural stiffnesses of the beam $k_\parallel$ and $k_\perp$.

$$\begin{pmatrix} F_x^1 \\ F_y^1 \end{pmatrix} = -\begin{pmatrix} k_\parallel & 0 \\ 0 & k_\perp \end{pmatrix}\begin{pmatrix} t_x \\ t_y \end{pmatrix} \qquad \text{where} \qquad k_\parallel = \frac{Eb\bar{H}}{L} \tag{3}$$

For a set of n fingers evenly placed around the device, the total force is then:

$$\begin{pmatrix} F_x \\ F_y \end{pmatrix} = -\sum_{i=0}^{n-1}\begin{pmatrix} \cos\frac{2\pi}{n} & \sin\frac{2\pi}{n} \\ -\sin\frac{2\pi}{n} & \cos\frac{2\pi}{n} \end{pmatrix}\begin{pmatrix} k_\parallel & 0 \\ 0 & k_\perp \end{pmatrix}\begin{pmatrix} \cos\frac{2\pi}{n} & -\sin\frac{2\pi}{n} \\ \sin\frac{2\pi}{n} & \cos\frac{2\pi}{n} \end{pmatrix}\begin{pmatrix} t_x \\ t_y \end{pmatrix} \tag{4}$$

If $n > 3$, the sum simplifies to an isotropic stiffness of $k = n(k_\parallel + k_\perp)/2$. If the fingers are not evenly spaced around the device, but can be partitioned into groups of symmetrical fingers, then this result still applies. Since $k_\parallel \gg k_\perp$ for a slender beam, a finger with average width $\bar{H}$ has a clamping stiffness of about:

$$k = \frac{nEb\bar{H}}{2L} \tag{5}$$

For our 8-finger devices and type II fingers, we get $k \approx 21$ N/μm. If we consider that the contact between the fingertip and its notch is frictionless, then a finger will pop out of its notch when the force it is transferring is equal to its clamping force. For our device, this limit occurs for a total force around 1 N, so the displacement of the grid when the fingers start sliding out of their notches is around 50 nm. Thus, as far as we are concerned, the grid is held in place rigidly. To put into perspective the 1 N maximum force on the grid, consider that the grid's mass is around 0.5 g, so the grid should be held in place for accelerations up to 200 g. Similarly, we can compute the rotational stiffness of the assembly; it is greater by a factor of 2, because in a rotation all the fingers are identically loaded along their axial direction. Finally, we must check that the fingers are not buckling or breaking. Indeed, we find that these failures occur for 100 N (from the Euler condition) and 35 N respectively, well after the fingertips have popped out of their notches.

III. Fabrication

We now describe the fabrication of the devices, which took place at the Microsystems Technology Laboratories (MTL) at MIT. Figure 8 shows the main steps in fabricating the device. Six devices are fabricated from two 6" diameter, double side polished, 650 μm thick silicon wafers. First a oxide is grown to protect the wafer surface for bonding, and alignment marks are patterned on both sides of each wafer (step 1). The *top* wafer is etched through with Deep Reactive Ion Etching (DRIE) to make the grids and grid supports of the device (step 2a). A recess is DRIE etched in the *bottom* wafer (step 2b), to be closer to an actual thruster, and to make recesses below the fingers that prevent the fingers from bonding to the bottom wafer. The bottom wafer is bonded to the top wafer, simulating the area where the needles are located, and providing alignment marks to evaluate the device (step 3). The completed devices are ready for hand assembly of the grid (step 4).

This process requires 3 photo-masks. One for all the alignment marks that appear on the device, one to describe the recess to be etched in the bottom wafer, and one to delineate the grid and grid support on the top wafer. Indeed, since the grids fit in the empty space inside the grid supports, we were able to combine the grids and grid supports on a single mask, removing a third of the processing steps. Six devices are placed on each 6" wafer, equally spaced around the outside of the wafer. The central region of the wafer is left empty to facilitate the onset of wafer bonding.

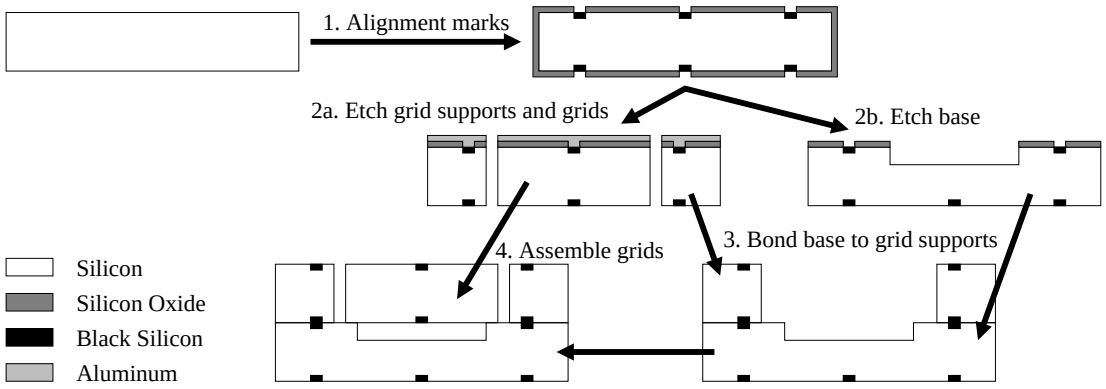

Figure 8. Fabricating the test device.

Finger geometry, base width (μm)	Maximum / assembled deflections (μm)	Post geometry
I. Tapered, 700	A. 50 / 25	8 circular posts
II. Straight, 550	B. 100 / 50	Complete ring
III. Tapered, 1000	C. 150 / 75	

Table 1. Finger geometry, deflection and post geometry were varied independently across dies.

To maximize our chances of getting working devices we introduced small variations between the devices (see Table 1, and Section II.A for details). Finger geometry was varied, trading off clamping force and maximum stress in the finger, and the grids were sized to cause varying amounts of deflection during assembly. At assembly time, any combination of finger geometry and deflection can be chosen because one is determined by the grid, and the other by the grid support. Finally, two different geometries were tried for the posts that support the grid in the vertical direction: small circular posts, and support that goes all around the device (in case the small posts get caught on grid features during assembly).

A. Process Details

Initially, all the wafers are processed identically. A protective oxide is grown on all the wafers to prevent scratches which could prevent wafer bonding. Then alignment marks are successively patterned on the front and back of each wafer. To pattern alignment marks on a side of the wafer, thin photo-resist is spun on both sides of the wafer, and one side is exposed to the alignment mark mask. After development, buffered oxide etchant (BOE) is used to etch through the oxide where the alignment marks should be, then a chlorine-based plasma treatment is used to blacken the underlying silicon. Finally, the photo-resist is stripped using an oxygen plasma and a piranha (H_2O_2/H_2SO_4 1:3) bath. After this initial preparation step, the wafers are separated into tops and bottoms, which undergo separate processing.

The bottom wafers are coated in thick photo-resist which is patterned with the desired recess shape. Then the exposed oxide is etched with BOE, and a recess about 100 μm deep is created using DRIE. At the end of the DRIE etch, a 30 second isotropic SF_6 etch is performed to smoothen the sidewall roughness and reduce the risk of crack formation.[13] Then the photo-resist is stripped with an oxygen plasma and piranha.

In designing the process, we were particularly careful to get the straightest possible side-walls for the grid and fingers, as it is the contact between the two that determines the precision of assembly. For this reason, we decided to use an aluminum etch mask when DRIE etching the top wafer. Indeed, aluminum is not measurably etched by the the DRIE process. By using it instead of thick photo-resist, we get better feature transfer from the optical mask, and avoid taper caused by resist thinning near the edge of features. First the wafer is coated in a layer of sputtered aluminum 0.2 μm thick. Then thin resist is spun on and patterned with the shape of the grids and grid supports. The outline of the pieces are defined using a 70 μm

trench. This improves etch uniformity and avoids plasma depletion by minimizing the amount of exposed silicon. The aluminum is etched with aluminum etchant "pan etch", and the underlying oxide with BOE. Then the wafer is mounted with photo-resist onto a quartz handler wafer. DRIE is used to etch through the wafer. Once the pieces have been cut out, and smoothed by an isotropic SF_6 etch, they are dismounted from the quartz wafer with acetone, and cleaned with an oxygen plasma and piranha.

Now we bond the top and bottom wafers together (except the grids, which are left aside). First, we clean the wafers using an oxygen plasma and piranha. Then we strip the protective oxide with hydrofluoric acid (HF), do an RCA clean (without HF) to minimize particulates. The wafers are then aligned, fusion bonded together, and annealed at 1050°C. Finally, the die saw is used to separate the 6 finished bases; they are ready for assembly.

IV. Experimental Results

A. Robustness

To date, one batch of 6 devices has been built, assembled and measured (Figure 9). The grids were assembled with the help of a small laser-cut plastic tool that engages the grid's assembly tool holes (Figure 7). The only unexpected difficulty was that two of the devices hadn't completely clicked into place (probably due to excess caution on our behalf). This lead to large misalignments (50 μm), but the source of the problem was clearly visible in an optical microscope; rotating the grid a bit more vigorously got it properly locked. The grid was easy to place in its recess, it rotated more or less easily depending on the grid and finger type. The finger robustness was satisfactory, with only four broken fingers: two side-by-side fingers when removing die-saw tape too fast, and one more during assembly for each type C grid (the ones with the largest deflection).[a] While it is true that the type C grid exceeds the design displacement by 50% for the type II and III fingers, our design was sufficiently conservative that we would not expect any breakage. Unfortunately, we did not try to assemble a type I finger (designed for a 150 μm displacement) with a type C grid, so we do not know if a finger would still have broken in that case.

Figure 9. An assembled grid with a broken finger.

During the design phase we did not think the grids could be disassembled without breaking fingers. Experimentally, disassembly has turned out to be straightforward. For the looser fits (type I or II finger with type A grid) we accidentally found that the grid can be successfully disassembled by rotating backward. Even better, we have found that for all the configurations, the grid can simply be pried up using a sharp object (this is easier to do when the grid is supported by posts – see Table 1). So far not a single finger has broken during disassembly despite dozens of attempts. We have also shown that a grid which has been partially pried up, but which is still engaged by all the fingers, can be pushed back down without any damage. This is an important observation as it could allow the grid to be rotated into place without interfering with the electrospray needles and then pushed down so the grid surrounds the needles as in Figure 10. This configuration is advantageous as it could lower startup voltage and allow a smaller hole size to be used for

[a]It is remarkable how consistent the single finger break has been on the type C grids; it also occurred on a few devices that were damaged during fabrication that we are not reporting in detail here.

a given beam divergence, which in turn would allow a tighter needle spacing.

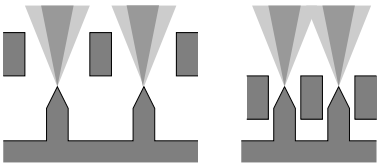

Figure 10. Lower grid permits denser needle packing for fixed beam divergence.

B. Precision of Assembly

We used an Electronic Vision Group TBM8 to measure the misalignment between alignment marks on the grid and corresponding marks on the back of the device. Marks were placed in the center and at four corners of the device so that both linear and angular alignment errors can be measured. (On most devices we only measured the center misalignment and one of the edge misalignments, after checking for a few cases that the five measurable misalignments were consistent with an isometry.) We made misalignment measurements on all six devices, repeating the measurement on some of the devices after a 3 months shelf period, and after disassembly/assembly cycles. We also repeated measurements multiple times consecutively to evaluate the measurement precision. Finally, we looked at the misalignment of the grid in the vertical direction for a few devices using an interferometric microscope, and found that the top of the grid is aligned with the top of the grid support to within a few micrometers.

Device	Conditions	θ (')	d_0 (μm)	$d_{\max}$ (μm)	Comment
3A	June 2005	-2.7	6.6	12.5	Grid III, finger I, ring, one broken finger
3A	September 2005	3.0	13.1	19.5	same
3A	After re-assembly	2.7	7.1	13.1	same
3A	Second re-assembly	2.5	13.6	19.1	same
3B	June 2005	-0.7	8.2	9.7	Grid II, finger III, ring, upside-down grid
3C	June 2005	0.1	9.6	9.8	Grid III, finger III, post, one broken finger
3C	September 2005	-1.3	1	3.9	same
3C	After re-assembly	-2.3	1.4	6.4	same
3C	Second re-assembly	-2.2	1.1	5.8	same
3D	June 2005	-1.4	8.5	11.5	Grid II, spring II, ring, two broken fingers
3E	June 2005	0.0	6.5	6.5	Grid I, spring I, post
3F	June 2005	-1.3	1.9	4.7	Grid I, spring II, post, upside down

Table 2. Misalignment measurement results. Upside down means that the grid was inserted upside-down compared with the grid holder (they originally came from the same wafer, which defines a common orientation).

The TBM8 has two roughly aligned cameras that look at the front and back of the device. By subtracting two measurements between which the device has been rotated 180°, any misalignment of the cameras is cancelled out, and we get a precise measure of the front-to-back misalignment on the device. A one pixel error when determining the alignment mark location corresponds to a 0.21 μm measurement error. When taking multiple measurements of the same misalignment, we have always found the same measurement to within 0.42 μm, which is a two pixel error. This error is negligible as far as we are concerned.

Table 2 summarizes the measurements that have been made. When multiple identical measurements were made, they are averaged before computing the values in the table. The reported values are θ, the angular misalignment, d_0, the misalignment distance at the center of the grid, and $d_{\max} = d_0 + r\,|\theta|$, the maximum misalignment across the central region of the grid which has a radius $r = 7.5$ mm. Because the grid is held in position by fingers at its periphery, we expect that if its size were increased, θ would decrease, and $d_{\max}$ would remain unchanged.

First we note that the precision of alignment is sufficient for the intended electrospray grid alignment application – beam divergence forces the grid holes to be have a diameter comparable with the wafer thickness (recall Figure 10), i.e., hundreds of micrometers in diameter, compared with less than 20 μm misalignment in the worst measured case. Moreover, broken fingers do not appear to reduce the alignment precision, even for two side-by-side broken fingers.

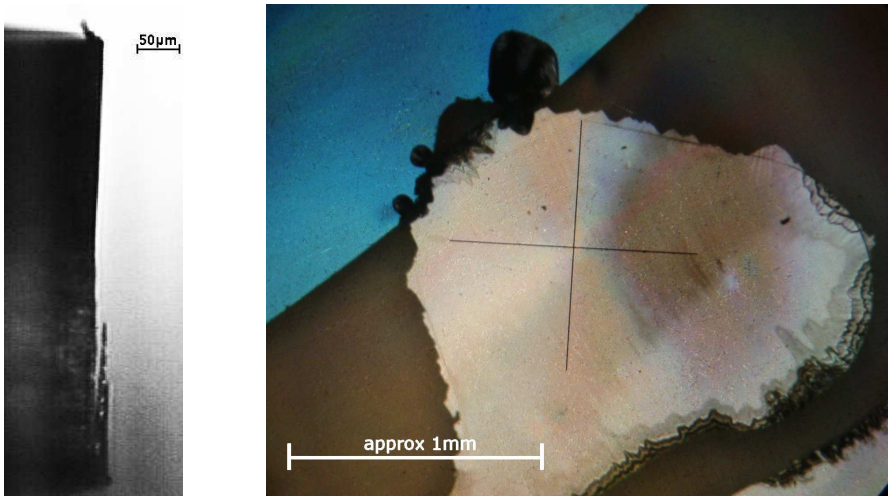

(a) Side-wall defects.

(b) A finger with jagged edges (center) engaged in its notch on the grid (top-left).

Figure 11. Some processing defects in the finished devices.

Comparing the measurements made in September 2005 with those made in June 2005 (with no intervening disassembly) shows that significant grid motion is taking place (5 to 10 μm). We do not know if this motion is spontaneous or is due to vibrations during handling. Since this variation is of the same order as the total misalignment error, we cannot expect to improve our alignment precision without finding the sources of this variation first. The same can be said of the misalignment that occurs when a device is reassembled.

The data collected so far is insufficient to pinpoint the sources of misalignment. As more devices are built, we will continue to collect data to try to find trends. Future revisions of the device should include alignment features that will allow misalignments to be determined directly from an optical microscope. This should speed up data collection which has been tedious with the TBM8. We can nevertheless comment on some possible sources of misalignment:

- When the alignment marks were originally patterned onto the wafers, a misalignment error of about 7 μm was introduced, due to the author's inexperience. Analyzing the measured misalignments suggests that this is not the only significant source of error, especially when the measurement variations for a single device are considered.
- When patterning the oxide on the top wafer, some of the photo-resist peeled off around the edges. This seems to have caused some unexpected roughness around the edges which may cause the fingers to lock away from their intended position in the notch. For future iterations of the process, we may strip the oxide on one side of the wafer before depositing the aluminum to avoid this problem. Figure 11(a) shows a side view of the DRIE etched sidewall with a stalagmite like structure rising from the bottom of the image.
- The through DRIE etch was ended a bit too early on the wafer we have been measuring. Consequently, the bottom of the trenches that delimit the grid and fingers was not completely cleared. This is visible in Figure 11(b), where the grid was mounted upside-down compared with the grid holder. One side is smooth, but the other has extra material a few micrometers thick. The extra material is fragile and breaks during assembly, possibly lodging itself at the interface between the fingertip and its notch.

Also, there seems to be some chipping at the surface of the grid around the notch. This chipping may be caused by the material that failed to clear in the DRIE etch.

All three of these problems are easy to solve for future iterations of the device, which will allow us to see whether they are actually dominating the observed misalignment error.

C. Electrical Testing

So far the device we have described has no electrical insulation between the base and the grid. Electrical insulation will be critical for a functional device, and we are currently working on ways to achieve it. Figure 12 shows three possible arrangements.

In Figure 12(a), we cover the silicon grids with a layer of LPCVD (low pressure chemical vapor deposition) silicon oxide, which should insulate the grid from the rest of the device. So far, when we performed this experiment, we were unable to avoid breakdown along the side-walls of the grid.

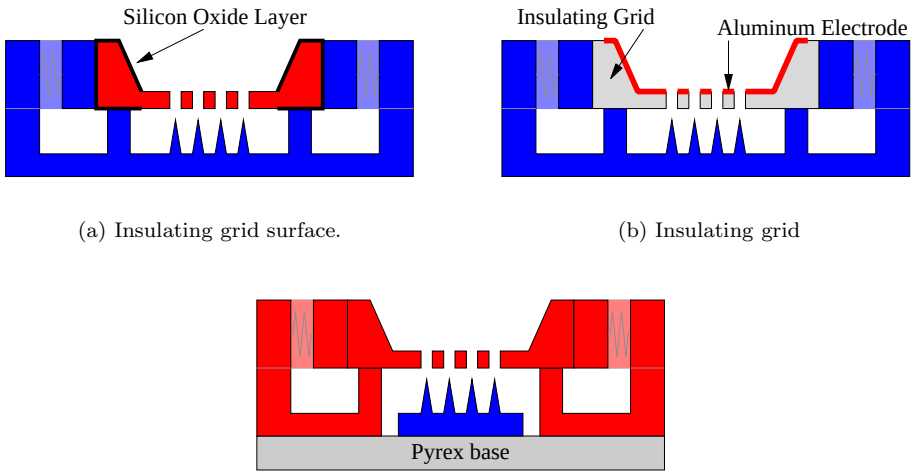

(a) Insulating grid surface.

(b) Insulating grid

(c) Insulating substrate

Figure 12. Three methods of electrically insulating the grid from the needles. Color indicates connected conductive regions.

We are also trying the method in Figure 12(b) in which the grid is made of an insulating material such as Pyrex or polyimide. A layer of sputtered aluminum serves as the extraction electrode. The shape of the grid will be cut out using a Resonetics laser cutter. The laser cutter will also remove aluminum near the edge of the grid to prevent any risk of shorting. These experiments with laser-cut grids should also give us an indication of how important side wall straightness is for alignment precision, and demonstrate the ease with which different grid materials can be tested. A downside to this method is that the insulating grid can collect charges during operation which could perturb the electric field and the electrospray process.

Another promising method which will require an additional mask, is to bond the bottom wafer to a Pyrex wafer and then etch a trench around the needles to insulate them from the rest of the silicon wafer. Now a large insulating gap can be provided without any insulating materials on the grid.

Once the electrical insulation has been demonstrated, we will still need to show that it can be maintained in the presence of the electrospray liquid. First, liquid for the electrospray must be confined to the region around the needles, even though the electric field tends to make the liquid want to close the electrical circuit. Also, we need to prevent stray emissions from coating the insulators and causing short circuits. Surrounding the needles with grid material as in Figure 10 could limit the range of the of the stray emissions.

V. Conclusion

We have presented the design and experimental validation of a method to mechanically assemble the grid of a micro-fabricated electrospray thruster array. In this method, the grid is assembled by hand by rotating it until cantilever springs called "fingers" engage in small notches. This method is particularly interesting as it decouples the fabrication of the grid and the rest of the thruster, permitting many different grid materials to be tried in the future, without making any changes to the process for the rest of the device.

In our experiments, once the grid is assembled, it is positioned within 20 μm of its intended location, which is sufficient for our application. Our method has proven its robustness: very few fingers broke during assembly, and missing fingers did not adversely affect the positional accuracy. In fact, we could disassemble the grids by prying them up without causing any damage. We conjecture that the misalignment we are observing is caused by processing problems that occurred when fabricating the first batch of our device.

In order to complete this work, we will need to demonstrate that the assembled grid can be electrically insulated from the rest of the thruster and support the multi-kilovolt extraction voltages that are necessary to start the electrospray, even in the presence of liquid that can potentially flow onto insulating surfaces and cause shorting.

Acknowledgments

This work was funded by the Air Force Office of Scientific Research, Mitat Birkan monitor, and by DARPA project BAA 040, Manager Clark T.-C. Nguyen, PhD. Also, B. Gassend would like to thank Prof. Srinivas Devadas for financial support while he was carrying out this work. Finally, we would like to thank the staff of the MIT Microsystems Technology Laboratories for all their support during the fabrication of these devices.

References

[1]Paine, M. and Gabriel, S., "A Micro-Fabricated Colloidal Thruster Array," *Proc. 37th AIAA/ASME/SAE/ASEE Joint Propulsion Conference and Exhibit*, No. 2001-3329, AIAA, Washington, DC, July 2001.

[2]Stark, J., Stevens, B., and Alexander, M., "Fabrication and Operation of Micro-Fabricated Colloid Thruster Arrays," *39th AIAA/ASME/SAE/ASEE Joint Propulsion Conference and Exhibit*, No. 2003-4852, AIAA, Washington, DC, July 2003.

[3]Velásques-García, L. F., Akinwande, A. I., and Martínez-Sánchez, M., "A Micro-fabricated Linear Array of Electrospray Emitters for Thruster Applications," JMEMS 1420, submitted to the *Journal of MicroElectroMechanical Systems*.

[4]Xiong, J., Zhou, Z., Sun, D., and Ye, X., "Development of a MEMS based colloid thruster with sandwich structure," *Sensors and Actuators A*, Vol. 117, 2005, pp. 168–172.

[5]Velásques-García, L. F., Akinwande, A. I., and Martínez-Sánchez, M., "A Planar Array of Micro-Fabricated Electrospray Emitters for Thruster Applications," JMEMS 1422, submitted to the *Journal of MicroElectroMechanical Systems*.

[6]Velásques-García, L. F., Akinwande, A. I., and Martínez-Sánchez, M., "Out-of-plane Wafer Assembly Using DRIE-patterned Spring Structures," JMEMS 1456, submitted to the *Journal of MicroElectroMechanical Systems*.

[7]Bostock, R. M., Collier, J. D., Jansen, R.-J. E., Jones, R., Moore, D. F., and Townsend, J. E., "Silicon Nitride Microclips for the Kinematic Location of Optic Fibers in Silicon V-Shaped Grooves," *Journal of Micromechanics and Microengineering*, Vol. 8, 1998, pp. 343–360.

[8]Last, M., Subramaniam, V., and Pister, K. S. J., "Out of Plane Motion of Assembled Microstructures using a Single-Mask SOI Process," *Proc. 13th International Conference on Solid-State Sensors, Actuators and Microsystems*, IEEE, New-York, June 2005.

[9]Prasad, R., Böhringer, K.-F., and MacDonald, N. C., "Design, Fabrication, and Characterization of SCS Latching Snap Fasteners for Micro Assembly," *Proc. ASME International Mechanical Engineering Congress and Exposition (IMECE)*, ASME, New-York, Nov. 1995.

[10]Lee, E., Kim, W., Song, I., Moon, C., Kang, M. K., Kim, H. C., and Chun, K., "A Morphology-Independent Wafer Level Rivet Packaging with Lego-Like Assembly," *Proc. 13th International Conference on Solid-State Sensors, Actuators and Microsystems*, IEEE, New-York, June 2005.

[11]Han, H., Weiss, L. E., and Reed, M. L., "Micromechanical Velcro," *Journal of MicroElectroMechanical Systems*, Vol. 1, No. 1, March 1992.

[12]Senturia, S., *Microsystem Design*, Springer, New-York, 2000.

[13]Chen, K.-S., Ayor, A., and Spearing, S. M., "Controlling and Testing Fracture Strength of Silicon on the Mesoscale," *Journal of the American Ceramics Society*, Vol. 83, No. 6, June 2000, pp. 1476–1484.